Considerations for Magnetic-Field Coupling Resulting in Radiated EMI

David Hockanson†, James L. Drewniak, Richard E. DuBroff, Todd H. Hubing, and Thomas P. Van Doren

† Sun Microsystems Computer Company, 901 San Antonio Road, MS MPK15-102, Palo Alto, CA 94303-4900, and University of Missouri–Rolla, 122 Department of Electrical Engineering, Electromagnetic Compatibility Laboratory, Rolla, MO 65409

Abstract: Parasitic inductance in printed circuit board geometries can worsen the EMI performance and signal integrity of high-speed digital designs. Partial-inductance theory is a powerful tool for analyzing inductance issues in signal integrity. However, partial inductances may not adequately model magnetic flux coupling to EMI antennas because the EMI antennas are typically open loops. Therefore, partial inductances may not always accurately predict radiated EMI from noise sources, unless used in a full-wave analysis such as PEEC. Partial inductances can be used, however, to estimate *branch inductances*, which can be used to predict EMI. This paper presents a method for decomposing loop or self inductances into branch inductances. Experimental as well as analytical investigations are used to compare branch- and partial-inductances.

I. Introduction

Equivalent circuits that effectively model the physics of EMI issues are desirable for EMI estimation at the design stage. Inductance may be decomposed into smaller pieces associated with the various conductors in a loop, the sum of which equals the total loop inductance. Partial-inductance theory has been successfully applied to analyze structures for signal integrity purposes. Magnetic-field coupling between traces and between pins in a high-density IC package, among others, have been analyzed using partial-inductance or partial-element theory [1], [2].

A method for decomposing loop inductance in a fashion that is useful for predicting EMI is presented herein. The decomposed inductance elements are called *branch inductances*. The branch inductance of a conductor models the magnetic flux that penetrates a conducting loop, and couples an EMI antenna. The branch inductance can then be used to model the resulting effective noise voltage that drives an EMI antenna. The branch-inductance model is presented herein, and compared with the partial-inductance theory. Two examples are investigated that demonstrate the difficulties in predicting EMI with partial inductances, and the advantage of branch inductances.

II. Concepts

The inductance of a conducting loop can be decomposed into parts that sum to the total loop inductance. In general, the decomposition is not unique. *Partial-inductance* theory was developed as a method for analyzing signal-integrity issues [3], [4], [5]. The formulation was extended into the Partial-Element Equivalent-Circuit (PEEC) method, which may be used to yield a full-wave equivalent-circuit model [6]. Loop inductance can also be decomposed into *branch inductances*, which are, in general, different from partial inductances. Branch-inductances are useful for determining the effects of EMI noise sources resulting from magnetic-field coupling.

Total inductance may be defined as the ratio of the magnetic flux that penetrates a loop to the current generating the magnetic flux as

$$L_{loop} \equiv \frac{\Psi_I}{I} = \frac{1}{I} \iint\limits_{S_{loop}} \mu \vec{\mathbf{H}} \cdot \vec{\mathbf{ds}} \tag{1}$$

The magnetic vector-potential $\vec{\mathbf{A}}$ is related to the magnetic field $\vec{\mathbf{H}}$ by $\vec{\mathbf{H}} \equiv \frac{1}{\mu} \nabla \times \vec{\mathbf{A}}$. Employing Stokes's theorem, the flux integral can be written in terms of a line integral,

$$L_{loop} = \frac{\Psi_I}{I} = \frac{1}{I} \iint\limits_{S_{loop}} \nabla \times \vec{\mathbf{A}} \cdot \vec{\mathbf{ds}} = \frac{1}{I} \oint\limits_{C} \vec{\mathbf{A}} \cdot \vec{\mathbf{dl}}. \tag{2}$$

A. Partial Inductance

Partial-inductance theory has been well documented [4], [5], [6], and is briefly reviewed here for completeness. The partial inductance of the i_{th} segment may be defined as the integral of the magnetic vector-potential along the i_{th} segment divided by the loop current I [5],

$$L^i_{partial} \equiv \frac{1}{I} \int\limits_{l_i} \vec{\mathbf{A}} \cdot \vec{\mathbf{dl}}. \tag{3}$$

The magnetic vector-potential used in this definition is the total magnetic vector-potential. The partial inductance of the i^{th} segment is therefore independent of conductors orthogonal to the i^{th} segment. The independence results because the magnetic vector-potential is oriented parallel to the current density. Consequently, $\vec{\mathbf{A}}_j \cdot \vec{\mathbf{dl}}_i = 0$ if the j^{th} and i^{th} segments are orthogonal to each other.

In addition to its generality, an advantage to Ruehli's formulation is that the resulting equivalent circuit model incorporates the mutual interactions among elements. Partial inductances are used to decompose the voltage drop associated with conductors in a loop that results from magnetic field storage. The partial inductance can be used to find the potential difference that results along

0-7803-5015-4/98/$10.00 © 1998 IEEE

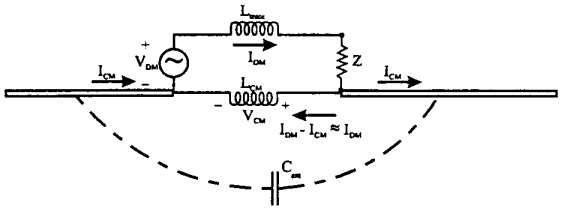

Figure 1. Schematic drawing showing the physics of a current-driven noise-source mechanism.

the conductors of the loop due to energy storage in the magnetic-field, which is useful for signal integrity models. However, the voltage drop modeled using the partial inductance concept is not necessarily the effective source that drives an EMI antenna. Partial inductance does not, in general, model the magnetic flux that may couple EMI antennas, because the magnetic vector potential is integrated only over the signal conductor. Partial-inductance theory can be used to approximate *branch inductances*. Branch inductance approximations may then be used to predict EMI.

B. Branch Inductance

Current-driven noise source-mechanisms in printed circuit designs are a consequence of high-frequency currents returning through reference structures of finite impedance [7], [8]. Flux wraps conductors of finite extent (transverse to current flow) and can lead to common-mode current on EMI antennas. Magnetic flux, or the storage of magnetic energy can be modeled schematically as an inductance. The resulting voltage drop can drive two portions of an extended conductor against each other as an EMI antenna. The EMI noise-source for a current-driven mechanism may be defined as $V_{CM} \approx L_{CM} \frac{d}{dt} I_{DM}$ as shown in Figure 1, where L_{CM} denotes the part of the total inductance associated with the signal-return conductor. The contribution of the vertical conductors to the total inductance is omitted. For EMI prediction, the inductance is decomposed into *branch inductances*, instead of partial inductances, therefore $L_{CM} = L_{branch}^{signal\ return}$ in Figure 1. Partial inductance is related to the voltage drop along conductors, which is useful for evaluating signal circuitry, but is not, in general, adequate for predicting EMI, because the partial inductance does not model all the magnetic flux that may couple to an EMI antenna. The definition for the branch inductance of the i^{th} segment of a conducting loop, is the net flux that mutually couples the conducting loop, and an open loop of which the i^{th} segment is part of the open loop boundary, divided by the current in the i^{th} segment, i.e.,

$$L_{branch}^{i} = \frac{\Psi_i}{I} = \frac{\begin{array}{c}\text{net flux coupling open loop} \\ \text{associated with Segment}i\end{array}}{\begin{array}{c}\text{amplitude of current} \\ \text{in Segment } i\end{array}}. \quad (4)$$

The open loops must be chosen such that the sum of the branch inductances is equal to the total inductance. Decomposing loop inductance into branch inductances assigns values based on how much magnetic flux couples regions external to the conducting loop.

An example of a simple wire circuit geometry is shown in Figure 2. The magnetic flux-lines depicted in Figure 2 have been distorted to aid discussion. The partial inductance of one of the vertical wires may be determined by integrating the magnetic vector-potential along the length of a vertical wire, and dividing by the current I [5]. The area external to the conducting loop can be divided into multiple regions, as shown in Figure 2 by the dotted lines $C1$, $C2$, $C3$, and $C4$. The open loop associated with the left vertical wire may be defined by the paths $C3$, the left vertical wire, and $C1$. The branch inductance of the left vertical wire segment may then be calculated by integrating the total magnetic vector-potential along those three paths, and dividing by the current I. The branch inductance of the remaining wire segments can be similarly calculated.

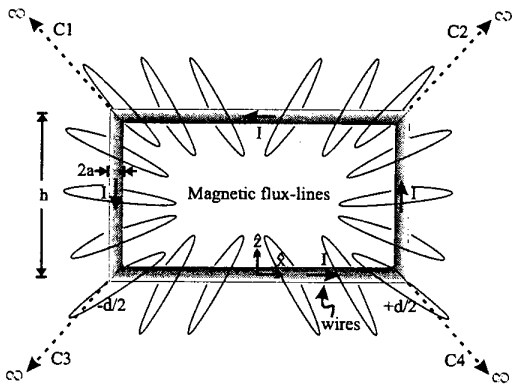

Figure 2. Simple wire loop showing magnetic flux lines.

Magnetic flux-lines are closed, therefore, the total magnetic flux penetrating the conducting loop must equal the total magnetic flux passing through the plane outside the conducting loop. Therefore, the sum of the branch inductances is equal to the total loop inductance. If the paths $C1$ through $C4$ are chosen such that the integration of the magnetic vector-potential is equal to zero along those paths, the branch inductance and the partial inductance are the same. Judiciously choosing the divisions of the area external to the conducting loop can yield branch inductance values that are useful for predicting EMI.

A parallel-plate example is illustrated in Figure 3. The parallel-plate example is used to demonstrate the suitability of the branch inductance for calculating the EMI noise source analytically and experimentally (see Section III-B). Two large plates (infinite in the $x-y$ plane for all practical purposes) are connected by two thin wires of length h. The partial inductance of the vertical wires in Fig. 3 is the same as the partial inductance of the vertical wires in Fig. 2. By the definition of partial inductance, changing the horizontal conductors to plates does not affect the partial inductance of the vertical conductors, because the plates are orthogonal to the vertical wires. However, the partial inductance of the horizontal plates is different from the horizontal wires for the configuration illustrated in Figure 3.

The partial inductance of the vertical conductors may be calculated using Eq. 3 or it may be found in a reference

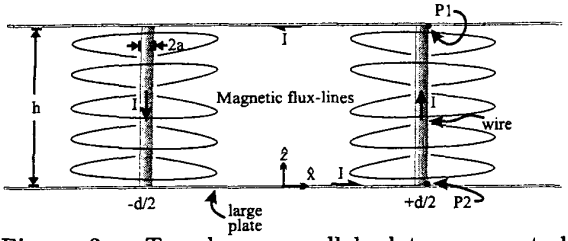

Figure 3. Two large parallel plates connected by two wires. Magnetic flux lines are shown wrapping the vertical wires.

such as Grover [3]. The partial inductance of the horizontal plate between the vertical wires may be calculated using Eq. 3, which yields

$$L_{partial}^{vertical\ wires} = \frac{\mu}{2\pi}\left[h\ln\left(\frac{d}{a}\right) - h\ \ln\frac{1}{2}\left(1+\sqrt{1+\frac{d^2}{h^2}}\right) - (h+d)+\sqrt{h^2+d^2}\right], \quad (5)$$

$$L_{partial}^{plate} = \frac{\mu}{2\pi}\left[h+d-\sqrt{h^2+d^2} + h\ln\frac{1}{2}\left(1+\sqrt{1+\frac{d^2}{h^2}}\right)\right], \quad (6)$$

where the separation between the wires and plates is assumed much greater than the wire radius. The total inductance of the conducting loop in Figure 3 is then,

$$L_{loop} = 2L_{partial}^{wire} + 2L_{partial}^{plate} = \frac{\mu}{\pi}h\ln\left(\frac{d}{a}\right). \quad (7)$$

The example shown in Figure 3 can also be treated using image theory. The wires connecting two conducting plates can be equivalently modeled as two infinitely long wires for calculating the fields between the two plates. The solution for the magnetic-field distribution between the plates for the image problem is the same as the solution for the non-image problem. The resulting expression for the loop inductance using image theory is the same as Eq. 7. However, the development using image theory shows more intuitively that no magnetic flux wraps the plates, because the magnetic vector-potential that results from image theory is oriented completely in $\hat{\mathbf{z}}$ direction. Therefore, $\vec{\mathbf{A}}\cdot\hat{\mathbf{x}}\,dx$ equals zero. Dividing the region external to the signal loop by the infinite plates and the vertical wires, the branch inductance of the plates is zero, and the branch inductance of each of the wires is half of the total inductance, by symmetry, i.e.,

$$L_{branch}^{plate} = 0 \quad (8)$$

$$L_{branch}^{wire} = \frac{\mu}{2\pi}h\ \ln\left(\frac{d}{a}\right) \qquad h, d \gg a. \quad (9)$$

The branch inductances of the wires and plates are, therefore, generally different from the partial inductances. However, as required by definition, the sum of all partial inductances comprising a loop equals the sum of all branch inductances comprising a loop, which is the total loop inductance,

$$L_{total}^{loop} = \sum_i L_{partial}^{i} = \sum_j L_{branch}^{j}. \quad (10)$$

The method for calculating and assigning partial inductances is very rigorous, however, some choices must be made when assigning branch inductances. Branch inductance calculations are useful for considering an EMI antenna and source geometry. The branch inductance of interest is associated with the conductor around which magnetic flux couples to the EMI antenna.

Partial inductance theory may be used to approximate branch inductance. For example, in Figure 3 the branch inductance of the right vertical wire could be computed with partial inductances, given the partial inductance of the top and bottom plates to the right of the loop are

$$L_{partial}^{P1\,\infty} = \frac{1}{I}\int_{P1}^{\infty}\vec{\mathbf{A}}(x,0,h)\cdot\hat{\mathbf{x}}\,dx \quad (11)$$

$$L_{partial}^{\infty\,P2} = \frac{1}{I}\int_{\infty}^{P2}\vec{\mathbf{A}}(x,0,0)\cdot\hat{\mathbf{x}}\,dx \quad (12)$$

The branch inductance of the right vertical wire in Figure 3 is

$$L_{branch}^{right\ vertical\ wire} = L_{partial}^{\infty\,P2} + L_{partial}^{vertical\ wire} + L_{partial}^{P1\,\infty}, \quad (13)$$

where $L_{partial}^{\infty\,P2}$, $L_{partial}^{vertical\ wire}$, and $L_{partial}^{P1\,\infty}$ are expressed in Eqs. 11, 5, and 12, respectively. The branch inductance can be calculated exactly as above, because the geometry is assumed to go to infinity. For typical PCB geometries of interest, the partial inductance approach to branch inductance can only be used to *approximate* the branch inductance. Partial inductances are calculated by integrating the magnetic vector-potential along the relevant conductors. Summing partial inductances, therefore, does not model the total magnetic flux to infinity that wraps conductors, as discussed previously in this section.

III. Comparative Investigations

Two experiments were conducted to demonstrate how branch inductance may be used to calculate effective EMI noise sources, when partial inductance may be inadequate. Measuring a partial or branch inductance directly is difficult. However, common-mode current can be directly related to the EMI noise source and can be measured with minimal disturbance to the DUT. A stacked-card configuration was investigated to demonstrate the difficulties of predicting EMI with partial inductances. A parallel-plate model was investigated to demonstrate how branch inductances, as opposed to partial inductances, may be used to predict EMI. The experimental models were constructed in a manner that permitted the measurement of common-mode current on a semi-rigid coaxial cable attached to the model. The common-mode current was measured using a clamp-on current probe and an HP8753D Network Analyzer. The measured common-mode current was directly proportional to $|S_{21}|$. For a complete description of the measurement procedure, the reader is referred to [8], [9].

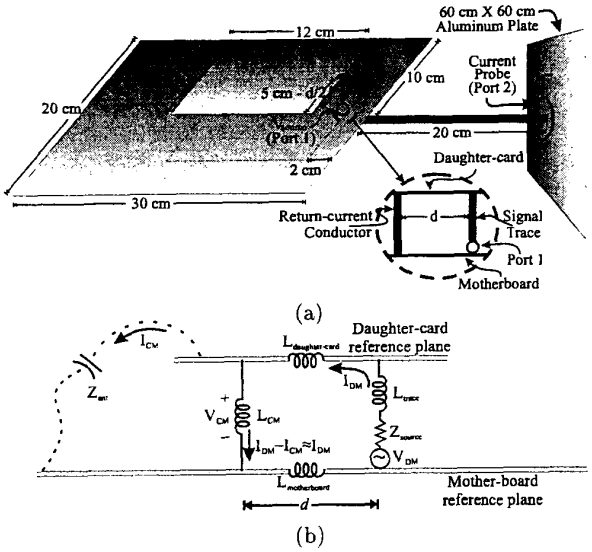

Figure 4. Stacked-card model (without traces) for investigating the common-mode current predicted by the partial- and branch-inductances. (a) Experimental model and (b) low-frequency equivalent circuit (cross-sectional view).

A. Stacked-Card PCB Model

Stacked-card and modules-on-backplane printed circuit-board geometries are advantageous for conserving real-estate in many designs. Unfortunately, at high frequencies, EMI resulting from the finite impedance of the signal return may develop at the connector. This effective noise source may drive the daughter-card against the mother-board and attached cables, resulting in common-mode radiation. A stacked-card model is shown in Figure 4(a). A model neglecting the trace geometry on the mother-board and daughter-card is desirable to investigate the role of the bus connector as an EMI noise source, assuming the trace geometry has little impact on the resulting EMI [9].

Port 1 was located between the mother-board and the signal conductor in the connector. The signal conductor was terminated directly to the daughter-card. The reference planes were constructed of single-sided electro-deposited copper on an *FR4* dielectric substrate. The cable extending from the mother-board was 0.085" semi-rigid coaxial cable. The cable was connected to the bottom of the mother-board and penetrated the mother-board at the signal conductor of the connector. The shield of the coaxial cable was soldered to the mother-board with a 360° connection. The center conductor of the coaxial cable was extended through the mother-board and connected to the daughter-card. A 24 *AWG* wire was used as the signal-return conductor a distance d from the signal conductor. The signal and return wires were located symmetrically with respect to the width of the daughter-card. The signal-return wire was soldered to the daughter-card and the mother-board reference-planes. The signal-input end of the coaxial cable was connected to the network

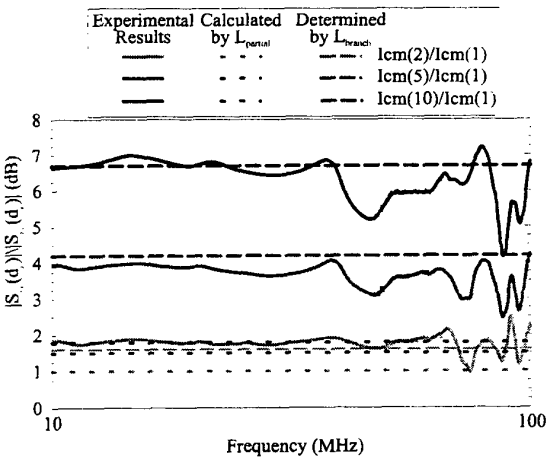

Figure 5. Results for the measured $|S_{21}|$ differences for d = *1 cm* & d = *2 cm*, d = *1 cm* & d = *3 cm*, and d = *1 cm* & d = *5 cm* for the stacked-card model.

analyzer through the aluminum plate as shown in Figure 4(a), and the common-mode current on the coaxial cable was measured. Swept-frequency measurements were made between *10 MHz* and *100 MHz*.

An equivalent circuit for the connector region of the stacked-card model is proposed in Figure 4(b). The EMI antenna impedance Z_{ant} is shown as a capacitor, which is a low-frequency model. The inductance of the signal loop in Figure 4 is decomposed into general inductances. The values of the decomposed inductances are dependent on the method of decomposition. A more thorough treatment of the stacked-card configuration may be found in [9].

$|S_{21}|$ was measured for the model shown in Figure 4(a) for signal return separations of d = *1 cm, 2 cm, 5 cm,* and *10 cm*. The partial inductance of the signal-return conductor with a signal return separation d was approximated using Eq. 5. The change in $L^{wire}_{partial}(d)$ with respect to $L^{wire}_{partial}(1\ cm)$ is compared to the average change in $|S_{21}(d)|$ with respect to $|S_{21}(1\ cm)|$. The results are tabulated in Table I, and are shown graphically in Figure 5. The changes in partial inductance are not consistent with the changes in $|S_{21}|$. The partial-inductance results do not agree well with the measurements, because the partial-inductance of the signal-return conductor does not account for where magnetic flux lines close. The magnetic flux is more likely to wrap small diameter wires, than large conducting plates. Therefore, the majority of the magnetic flux lines wraps the wires. The magnetic flux is approximately equally distributed between the signal and return conductors, because of the symmetry of the connector. The branch inductance of the signal-return conductor may then be defined as all the magnetic flux that wraps the signal-return conductor. A closed-form expression for the branch inductance of the signal-return conductor is not available, because of the complicated current distribution on the daughter-card and mother-board. However, the branch inductances of the signal loop can be determined from measurements,

TABLE I

CALCULATED PARTIAL INDUCTANCE RESULTS AND BRANCH INDUCTANCE RESULTS EXTRACTED FROM MEASUREMENTS FOR d = *1 cm, 2 cm, 5 cm,* AND *10 cm* FOR THE STACKED-CARD CONFIGURATION. THE CHANGE IN PARTIAL AND BRANCH INDUCTANCE WITH RESPECT TO $L^{wire}_{partial}(1\ cm)$, AND $L^{wire}_{branch}(1\ cm)$, RESPECTIVELY, IS GIVEN IN DECIBELS, AND CONTRASTED TO THE AVERAGE CHANGE IN $|S_{21}|$.

Results for Signal-Return Conductor in Stacked-Card Configuration					
d (cm)	$L^{wire}_{partial}(d)$ (nH)	$\frac{L^{wire}_{partial}(d)}{L^{wire}_{partial}(1\ cm)}$ (dB)	$L^{wire}_{branch}(d)$ (nH)	$\frac{L^{wire}_{branch}(d)}{L^{wire}_{branch}(1\ cm)}$ (dB)	$\left(\frac{\lvert S_{21}(d)\rvert}{\lvert S_{21}(1\ cm)\rvert}\right)$ (dB)
1	12.9	0	17.5	0	0
2	14.4	1.0	21.0	1.6	1.7
5	15.4	1.5	28.5	4.2	3.7
10	15.8	1.8	38.0	6.7	6.4

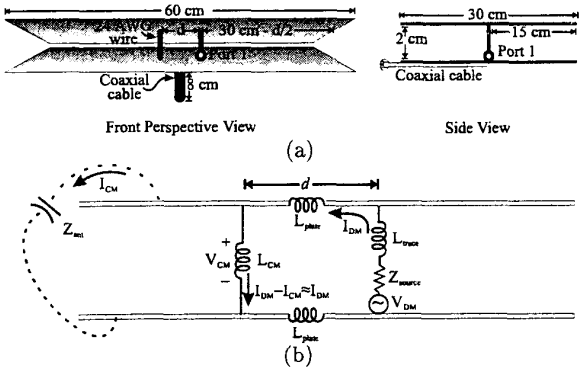

Figure 6. Parallel-plate model for investigating the common-mode current predicted by the partial-and branch-inductances. (a) Experimental model and (b) low-frequency equivalent circuit (cross-sectional view).

assuming that the branch inductance of the wires is one half of the total loop inductance. The branch inductance was calculated as half of the total loop inductance, which was measured with an HP 4291A Impedance/Material Analyzer *(1 MHz - 1.8 GHz)*. The change in common-mode current predicted using branch inductance agrees well, in general, with the measured change. The peaks and valleys shown in Figure 5 result from slight shifts in the measurement parasitics when the connector geometry was changed. However, the differences between the experimental results shown in Figure 5 are consistent over the measured frequencies. For example, $|S_{21}(5)|/|S_{21}(1)|$ appears approximately *2 dB* greater than $|S_{21}(2)|/|S_{21}(1)|$ over the measured bandwidth.

B. Parallel-Plate Model

An analytical expression for the branch inductance of the stacked-card geometry is not easily derived. However, an analytical expression was developed for the branch inductance of a vertical wire between two large plates [9]. A schematic representation of a parallel-plate configuration is shown in Figure 6(a). The plates of the model are necessarily finite, but large enough that the the magnetic field distribution between the plates is approximately the same as for the infinite plate case. The plates were constructed of RT-Duroid single-sided copper-clad boards. The vertical wires were 24 AWG wire. A 0.085" semi-rigid coaxial cable was used to excite the differential-mode loop, and to return common-mode current for measurement. The coaxial cable extended *8 cm* from the bottom plane, and was parallel to the planes. The wire separation d varied from d = *1 cm, 5 cm,* and d = *10 cm*. The location of Port 1 was shifted for each separation d to maintain symmetry with respect to plate edges, and limit possible artifacts resulting from the proximity of the plate edge. A low-frequency equivalent circuit-model is shown in Figure 6(b). The equivalent circuit shown in Figure 6(b) shows a current-driven noise source-mechanism that results in a potential difference between the top and bottom plates. The EMI antenna impedance Z_{ant} is shown as a capacitor, which is a low-frequency model. The loop inductance in Figure 6 is decomposed into general inductances. The value of the decomposed inductances is dependent on the method of decomposition. The branch inductance of the two plates is zero as discussed in Section II-B, although the partial inductance of the two plates is finite and non-zero.

The common-mode current was measured via $|S_{21}|$ measurements using the network analyzer. The increase in common-mode current is predictable with a common-mode inductance model, such as shown in the equivalent circuit diagram of Figure 1. The partial and branch inductances for a wire in the parallel-plate geometry were calculated using Eq. 5 and Eq. 9, respectively. The increase in common-mode current predicted by the two decomposed inductance models was compared to the increase in $|S_{21}|$. The results are tabulated in Table II, and are shown graphically in Figure 7. The measured results show fair agreement with the change in common-mode current predicted using branch inductances. The valleys and peaks in Figure 7 result from small changes to the measurement system when the wire separation was changed. The ratio of the common-mode current with d =*5 cm* to d = *10 cm* shows the same valleys and peaks with an average difference of *1.1 dB*. The valleys and peaks may be discerned in the $|S_{21}|$ plots, as well. The change in common-mode current predicted using partial inductance does not agree well with the measurements. The partial-inductance theory does not model the magnetic flux that couples the EMI antenna, because the partial inductance is calculated by integrating the magnetic vector-potential over a finite length. Consequently, the partial inductance of the vertical wires can not be used to accurately predict the level of the common-mode voltage-source for the geometry shown in Figure 6.

TABLE II

CALCULATED PARTIAL INDUCTANCE AND BRANCH INDUCTANCE RESULTS FOR $d = 1\ cm$, $5\ cm$, AND $10\ cm$ FOR THE PARALLEL-PLATE CONFIGURATION. THE CHANGE IN PARTIAL AND BRANCH INDUCTANCE WITH RESPECT TO $L^{wire}_{partial}(1\ cm)$, AND $L^{wire}_{branch}(1\ cm)$, RESPECTIVELY, IS GIVEN IN DECIBELS, AND CONTRASTED TO THE AVERAGE CHANGE IN $|S_{21}|$.

Results for Signal-Return Conductor in Parallel-Plate Geometry					
d (cm)	$L^{wire}_{partial}(d)$ (nH)	$\frac{L^{wire}_{partial}(d)}{L^{wire}_{partial}(1\ cm)}$ (dB)	$L^{wire}_{branch}(d)$ (nH)	$\frac{L^{wire}_{branch}(d)}{L^{wire}_{branch}(1\ cm)}$ (dB)	$\left(\frac{\lvert S_{21}(d)\rvert}{\lvert S_{21}(1\ cm)\rvert}\right)$ (dB)
1	12.9	0	14.7	0	0
5	15.4	1.5	21.1	3.1	3.0
10	15.8	1.8	24.0	4.2	4.1

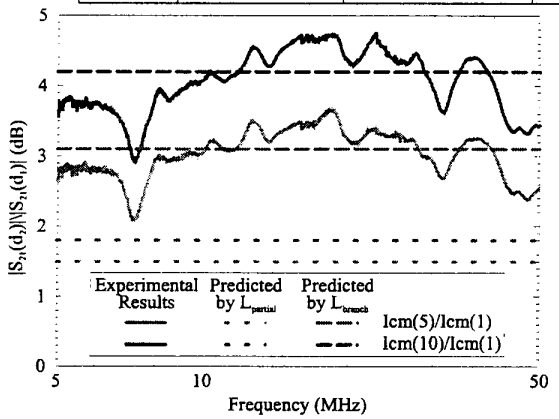

Figure 7. Results for the measured $|S_{21}|$ differences for $d = 5\ cm$ & $d = 1\ cm$, and $d = 10\ cm$ & $d = 1\ cm$ for the parallel-plate model.

IV. SUMMARY

Equivalent circuit models are useful tools for understanding and predicting EMI. The concept of branch inductance was presented and studied herein as a means for decomposing loop inductance. Branch inductance models the magnetic flux coupling the differential-mode loop and an open region adjacent to the loop. Consequently, the magnetic flux coupling to EMI antennas is incorporated in the signal circuit-model and the level of common-mode noise-voltage can be predicted. The open region necessary for computing the branch inductance is arbitrary, however, and the user must judiciously choose the region to model the magnetic flux that can excite the EMI antenna. Partial-inductance theory was reviewed and found to be unsuitable for predicting common-mode noise, although it is accepted as a powerful tool for analyzing signal integrity issues. The loop comprising the EMI antenna is generally an open loop. Therefore, the partial-inductance values associated with the EMI antenna are not sufficient for determining the total magnetic flux that is mutually coupling the signal circuit and the EMI antenna. A complete PEEC (full-wave) model could, however, be used to investigate EMI. A stacked-card configuration and a simple parallel-plate configuration were analyzed to contrast the resulting common-mode current predicted by partial-and branch-inductances. The predicted levels were compared to measured results. The branch-inductance method for decomposing loop inductances was found to predict the changes in common-mode current reasonably well.

V. ACKNOWLEDGEMENTS

The authors are very grateful to Al Ruehli for his helpful correspondence.

REFERENCES

[1] M. Kamon, M. J. Tsuk, and J. K. White, "FASTHENRY: A multipole-accelerated 3-D inductance extraction program", *IEEE Transactions on Microwave Theory and Techniques*, vol. 42, pp. 1750–1757, 1994.

[2] L. M. Silveira, M. Kamon, and J. White, "Efficient reduced-order modeling of frequency-dependent coupling inductances associated with 3-D interconnect structures", *IEEE Transactions on Components, Packaging, and Manufacturing Technology–Part B*, vol. 19, pp. 283–288, 1996.

[3] H. W. Grover, *Inductance Calculations: Working Formulas and Tables*, Dover Publications, New York, New York, 1962.

[4] A. E. Ruehli, "Inductance calculations in a complex integrated circuit environment", *IBM Journal of Research and Development*, vol. 16, pp. 470–481, 1972.

[5] C. R. Paul, *Introduction to Electromagnetic Compatibility*, John Wiley & Sons, Inc., New York, New York, 1992.

[6] A. E. Ruehli, "Equivalent circuit models for three-dimensional multiconductor systems", *IEEE Transactions on Microwave Theory and Techniques*, vol. MTT-22, pp. 216–221, March 1974.

[7] D. M. Hockanson, J. L. Drewniak, T. H. Hubing, T. P. Van Doren, Fei Sha, and M. Wilhelm, "Investigation of fundamental EMI source mechanisms driving common-mode radiation from printed circuit boards with attached cables", *IEEE Transactions on Electromagnetic Compatibility*, pp. 557–566, November 1996.

[8] D. M. Hockanson, J. L. Drewniak, T. H. Hubing, T. P. Van Doren, Fei Sha, C.-W. Lam, and L. Rubin, "Quantifying EMI noise sources resulting from finite-impedance reference planes", *IEEE Transactions on Electromagnetic Compatibility*, pp. 286–297, November 1997.

[9] D. M. Hockanson, *An Investigation of Coupling Mechansisms on Printed Circuit Boards Leading to Electromagnetic Interference*, PhD thesis, University of Missouri–Rolla, 1997.